Asymptotically Stable Walking and Steering of a 3D Bipedal Robot with Passive Point Feet

Ching-Long Shih, *Member, IEEE*, J. W. Grizzle, *Fellow, IEEE*, and Christine Chevallereau

***Abstract*— This paper presents a hybrid feedback controller that achieves an asymptotically stable walking gait for a 3D bipedal robot with unactuated point feet. In addition to walking along a straight line, the controller is capable of adjusting the net yaw rotation of the robot over a step in order to steer the robot along paths with mild curvature. The studied robot is composed of 5-links and has 9 DoF (degree-of-freedom) in the single support phase and six actuators. The nominal hybrid controller consists of a time-invariant within-stride controller that creates a periodic walking motion and stabilizes all but the yaw motion of the robot about the stance foot, and an event-based (or stride-to-stride) controller that stabilizes the yaw motion and provides steering. The event-based feedback law automatically distributes set-point changes to all of the actuated joints in order to achieve a desired amount of turning. An interesting feature of this work is that one is able to control the robot's motion along a curved path using only a single predefined periodic motion.**

***Index Terms*—3D underactuated bipedal robot, hybrid zero dynamics, orbital stability, Poincaré map, steering, stride-to-stride control**

I. Introduction

IN a previous paper, we addressed the control of a 3D bipedal robot with point feet, where the ground contact inhibited yaw motion, but pitch and roll were unconstrained and unactuated. Such contact conditions arise naturally as the limiting case when the surface area of the support foot tends to zero. The first objective of this paper is to remove the restriction on yaw and allow a completely unconstrained and unactuated 3D point foot contact model. The second objective of the paper is to present an event-based controller that steers the robot along paths of low curvature. A novel feature of the solution is that steering is achieved on the basis of a single, predefined, periodic motion corresponding to walking along a straight line.

Manuscript received June 5, 2009. This work of C.-L. Shih was supported by the Taiwan National Science Council (NSC) under Grant NSC 97-2212-E-011-062. The work of J.W. Grizzle is supported by NSF grant ECS-0600869.

C.-L. Shih is with the Department of Electrical Engineering, National Taiwan University of Science and Technology, 106, Taipei, Taiwan (e-mail: shihcl@ntust.edu.tw).

J. W. Grizzle is with Control System Laboratory, Department of Electrical Engineering and Control Science, University of Michigan, Ann Arbor, MI 48109-2122 USA. (e-mail: grizzle@umich.edu).

Christine Chevallereau is with the IRCCyN, CNRS, Ecole centrale de Nantes, 1 rue de Noe, 44321 Nantes, codex 03, France (e-mail: Christine.Chevallereau@irccyn.ec-nantes.fr).

Research on bipedal walking can be roughly divided along the degree of actuation throughout the gait (full actuation versus underactuation), and whether walking motions are along a straight line or turning is considered. Comments will be limited to 3D bipedal robots.

For walking in a straight line, the analysis of passive (i.e., unactuated) 3D bipeds is presented in [6] and references therein. A model with a passive contact at the leg end, passive dynamics in the sagittal plane and sufficient actuation in the fontal plane in order to regulate step width was presented in [12]; stable walking was demonstrated by estimating the eigenvalues of the Jacobian of the Poincaré map. The emphasis in [6] and [12] is on energy efficiency through "natural dynamics" and not on feedback control for achieving a wide range of behaviors. For a biped with a passive point foot contact and all other joints actuated, the method of virtual constraints [9, 21] was applied in [7] to regulate the sagittal plane motion of a walking gait, while an inverted pendulum approximation of the dynamics was used to design a controller for the frontal plane; an event-based controller was then used to synchronize the frequency of the sagittal and frontal plane controllers. In [18], the control for a similar robot was designed on the basis of linearizing the robot's model along a periodic orbit; so that the controller would be time-invariant, the orbit was parameterized with a configuration variable that is strictly monotonic throughout a normal gait, as in [3, 9, 15, 21], before linearization was applied. In [7] and [18], the robots can execute walking gaits on flat ground, but formal proofs of stability are lacking.

In order to address stability and to provide a large basin of attraction, [19] assumed full actuation (i.e., actuation between the leg end and the ground, in addition to all internal joints of the robot being actuated). It was shown that passive 3D gaits that exist on sloped ground could be realized on flat ground by "shaping" the potential energy of the robot via feedback control. A much wider class of 3D walking gaits is being developed in [28], [1], [29] and [30], along with formal methods for establishing stability, under the hypothesis of full actuation. A method called "hybrid Routhian reduction" has been developed that allows the sagittal and frontal plane dynamics of a 3D biped to be decomposed in a rigorous manner. A key outcome is that walking gaits of the sagittal plane portion of the robot's model can be lifted to the full 3D model; moreover, stability can be established by estimating the eigenvalues of the Jacobian of the Poincaré map. The assumption of full actuation at the leg end entails flat-footed walking. Very recently, a result that allows underactuation in the sagittal plane has been reported in [31] and [32]; in particular, the studied gait allows

heel strike, a flat-footed phase, and toe roll, with the first and last phases being underactuated. Actuation at the foot in the direction of the frontal plane is still assumed in all phases, as opposed to the completely unactuated assumption made here.

The ability to turn is an essential feature for stepping around obstacles on a given surface. Honda's AISMO has demonstrated the important ability to walk forward, backward, right, left, up and down stairs, and on uneven terrain [16]. Very few other works have addressed the issue of a turning motion for bipedal robots, and all addressed models with actuated feet [11, 13, 24] (in particular, full actuation was assumed). Previous techniques on bipedal turning motion include change of the duty ratios of the two legs, slipping the feet on the ground, reduction and decoupling, and trial-and-error methods. For instance, by adjusting the swing leg center of mass and hip position trajectories in a trial and error fashion, it is possible to maintain the robot's stability during turning [24]. Generating a turning motion of a bipedal robot by slipping the feet on the ground was presented in [13]. To generate the slip motion, the authors predict the amount of slip using the hypothesis that the turning motion is caused by the effect of minimizing the power generated by floor friction. It has been shown that straight line and turning walks could be realized by nonlinear oscillator systems, and the turning motion leads to the change of the duty ratios of the legs [11]. The authors of [8, 25-27] have developed an elegant and rigorous setting for stable walking and steering of fully actuated 3D robots on the basis of geometric reduction and passivity-based control. The controlled geometric reduction decouples the biped's sagittal-plane motion from the yaw and lean modes. Passivity-based control is used to create and stabilize planar limit cycles that arise from the sagittal component of the reduction. Steering is achieved by adjusting the yaw set point of the within-stride passivity-based controller.

We study here a 3D passive point contact at the leg end, and, for a 5-link robot, seek a time-invariant feedback controller that creates an exponentially stable, periodic walking motion, along with the ability to steer the yaw orientation of the robot with respect to an inertial frame, that is, the robot's direction of travel. In our previous studies on 3D bipedal robots, we assumed a model where the ground contact inhibited yaw motion, but pitch and roll were unconstrained and unactuated. Starting with a simple 3-link model [17] and followed by a 5-link model [5], we used the techniques of virtual constraints [9], hybrid zero dynamics [21, 14] and event-based control [10] to achieve exponentially stable, periodic walking motions. The primary goal in the present study is to design and stabilize periodic orbits for a 3D bipedal robot with point feet modeled as a passive three degree of freedom pivot. The control approach presented in this paper allows us to change the direction of motion of the robot through the net yaw motion about the stance foot over a step. An event-based (or stride-to-stride) feedback controller distributes set point commands to the actuated joints in order to achieve a desired amount of turning, as opposed to the continuous corrections used in [25].

Section II presents the dynamic model of the biped; it is hybrid due to the assumption of inelastic impacts. An important symmetry of the model is noted [19] which well be exploited in the control design. Section III summarizes the framework for simultaneous gait and within-stride controller design. Stability analysis of periodic orbits is presented in Section IV, for both the full dynamic model and for a restricted model based on hybrid zero dynamics. In Section V, simulation results of walking along a straight line are studied; it is noted that the yaw motion about the stance foot is unstable under the within-stride controller. A supplemental event-based control law to stabilize the yaw motion is proposed. In Section VI, it is shown how the event-based controller can be easily modified in order to steer the robot by regulating the net yaw motion about the stance foot over a step. Several simulation results are presented. Section VII concludes the paper.

II. MODEL

A. Description of the Robot

The 3D bipedal robot discussed in this work is shown in Fig. 1. It consists of five links: a torso and two legs with knees that are terminated with "point-feet." Each hip consists of a revolute joint with 2 degrees of freedom and each knee is formed by a 1 degree of freedom revolute joint. These six joints (three in each leg) are independently actuated. The stance leg end is assumed to act as a passive pivot, so the leg end is modeled as a point contact with 3 degrees of freedom and no actuation. In total, the biped in the single support phase has 9 degrees of freedom, and there are hence 3 degrees of underactuation.

The following assumptions are made in this study:

(1) Each link is rigid and has mass.
(2) Walking consists of two alternating motion phases: single support and double support.
(3) The double support phase is instantaneous and involves the impact of the swing leg with the ground.
(4) At impact, the swing leg neither slips nor rebounds.
(5) The swing and stance legs exchange their roles at each impact.
(6) Walking takes place on a flat surface.

Since the gait is composed primarily of single support phases, the variables used to describe the robot are adapted to this phase of motion. Assuming support on leg 1, a set of generalized coordinates $q = [q_0, q_1, \cdots, q_8]^T$ is shown in Fig. 1. Angles (q_0, q_1, q_2) are yaw, roll and pitch angles of the stance leg, respectively, relative angle q_3 is the flexion-extension of the stance knee, relative angles (q_4, q_5) are the flexion-extension and the adduction-abduction of the stance hip respectively. Relative angles (q_6, q_7) are the adduction-abduction and the flexion-extension of the swing hip respectively, and relative angle q_8 is the flexion-extension of the swing knee. The coordinates (q_0, q_1, q_2) are unactuated (passive contact), while $(q_3, q_4, \cdots, q_8)$ are independently actuated (active joints). The position of the robot with respect to an inertial frame is defined by adding three variables to q in order to form $q_e = [q^T x_1 \; y_1 \; z_1]^T$, where (x_1, y_1, z_1) are the Cartesian coordinates of the stance foot, which are constant during each single support phase. When leg 2 is the stance leg, then a new set of generalized coordinates q is defined as shown in Fig. 2,

and the same notation is employed as when leg 1 is the supporting leg.

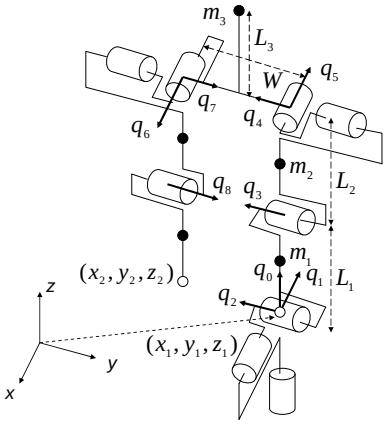

Fig. 1. A 3D point-feet bipedal robot when support on leg 1, the 3 degrees of freedom at the leg end are unactuated. For simplicity, each link is modeled by a point mass at its center.

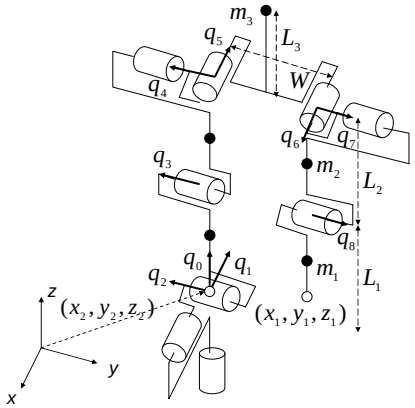

Fig. 2. The generalized coordinates of the bipedal robot when support on leg 2.

B. Dynamic Model and the Walking Gait

The dynamic models for single support and impact (i.e. double support) are derived here assuming support on leg 1. The models for support on leg 2 can be written in a similar way by using a hip width of –W in place of W, which then places the swing leg on the correct side of the stance leg. The Euler-Lagrange equations yield the dynamic model for the robot in the single support phase as

$$D(q)\ddot{q} + C(q,\dot{q})\dot{q} + N(q) = Bu = \begin{bmatrix} 0_{3\times 6} \\ I_{6\times 6} \end{bmatrix} u \,, \tag{1}$$

where $D(q)$ is the positive-definite (9×9) mass-inertia matrix, $C(q,\dot{q})$ is the (9×9) Coriolis matrix, $N(q)$ is the (9×1) gravity vector, B is an (9×6) full-rank, constant matrix indicating whether a joint is actuated or not, and u is the (6×1) vector of input torques.

Following standard practice in the literature, the double support phase is assumed to be instantaneous. However, it actually consists of two distinct subphases: the impact, during which a rigid impact takes place between the swing foot and the ground, and coordinate relabeling, which is responsible for switching the roles of the two legs after the impact so that same dynamic model can be applied in the single support phase [9].

During the impact, the biped's configuration variables do not change, but the generalized velocities undergo a step change. The derivation of the impact model in double support phase requires using the extended set of generalized coordinates $q_e = [q^T x_1\ y_1\ z_1]^T$. Conservation of momentum during the impact process and the swing leg neither slipping nor rebounding at impact yield

$$D_e(\dot{q}_e^+ - \dot{q}_e^-) = E_2^T F_2 \tag{2}$$

and

$$E_2 \dot{q}_e^+ = 0\,; \tag{3}$$

therefore,

$$\begin{bmatrix} \dot{q}_e^+ \\ F_2 \end{bmatrix} = \begin{bmatrix} D_e & -E_2^T \\ E_2 & 0_{3\times 3} \end{bmatrix}^{-1} \begin{bmatrix} D_e \dot{q}_e^- \\ 0_{3\times 1} \end{bmatrix}, \tag{4}$$

where $\dot{q}_e^-$ and $\dot{q}_e^+$ are the extended velocities before and after the impact, respectively, F_2 is the impulsive reaction force at the contact point, D_e is the extend mass-inertia matrix, and $E_2 = \frac{\partial}{\partial q_e}[x_2\ y_2\ z_2]^T$ is the Jacobian matrix for the position of the swing foot of leg 2.

The support-swing leg swapping and relabeling take place immediately after the impact of the swing foot. Immediately after the impact, leg 2 will be the new stance leg and a new set of generalized coordinates q and $q_e = [q^T x_2\ y_2\ z_2]^T$ is then used to describe the robot motion. Let R and $\omega = [\omega_1 \quad \omega_2 \quad \omega_3]^T$ be the rotational matrix and the angular velocity of the shin of leg 2 just after the impact. R and ω can be expressed with the set of coordinates used to describe the support on leg 2 (see Fig. 2). We have

$$R_z(q_0^+)R_x(-q_1^+)R_y(-q_2^+) = R \tag{5}$$

or

$$\begin{bmatrix} c_0c_2 - s_0s_1s_2 & -s_0c_1 & -c_0s_2 - s_0s_1c_2 \\ s_0c_2 + c_0s_1s_2 & c_0c_1 & -s_0s_2 + c_0s_1c_2 \\ c_1s_2 & -s_1 & c_1c_2 \end{bmatrix} = R\,,$$

where $R_x(\cdot)$, $R_y(\cdot)$ and $R_z(\cdot)$ are the three basic rotational matrices with respect to x-axis y-axis and z-axis, respectively; one can obtain

$$q_0^+ = \text{atan2}(-R_{1,2}, R_{2,2}) \tag{6}$$

$$q_1^+ = \text{atan2}(-R_{3,2}, -s_0R_{1,2} + c_0R_{2,2}) \tag{7}$$

$$q_2^+ = \text{atan2}(-c_0R_{1,3} - s_0R_{2,3}, c_0R_{1,1} + s_0R_{2,1}) \tag{8}$$

and

$$\begin{bmatrix} \dot{q}_0^+ \\ \dot{q}_1^+ \\ \dot{q}_2^+ \end{bmatrix} = \begin{bmatrix} 0 & -c_0 & s_0c_1 \\ 0 & -s_0 & -c_0c_1 \\ 1 & 0 & s_1 \end{bmatrix}^{-1} \begin{bmatrix} \omega_1 \\ \omega_2 \\ \omega_3 \end{bmatrix}, \tag{9}$$

where $c_i = \cos(q_i^+)$ and $s_i = \sin(q_i^+)$, $i = 0,1,2$.

Analogously to [5], the overall impact model is written as

$$q^+ = \Delta_q(q^-) \tag{10}$$

and

$$\dot{q}^+ = \Delta_q(q^-, \dot{q}^-)\,, \tag{11}$$

where $(q^-,\dot{q}^-)$ are joint angles and joint velocities of the bipedal robot for support on leg 1 just before the impact; and $(q^+,\dot{q}^+)$ are joint angles and joint velocities of the bipedal robot for support on leg 2 and immediately after the impact.

Define state variables $x_j = \begin{bmatrix} q \\ \dot{q} \end{bmatrix}$, and let $x_j^+ = \begin{bmatrix} q^+ \\ \dot{q}^+ \end{bmatrix}$ and $x_j^- = \begin{bmatrix} q^- \\ \dot{q}^- \end{bmatrix}$, where the subscript $j \in \{1,2\}$ denotes the stance leg number. Then a complete walking motion of the robot can be expressed as a nonlinear system with impulse effects, as shown in Fig. 3 and written as

$$\Sigma: \begin{cases} \dot{x}_1 = f_1(x_1) + g_1(x_1)u_1 & x_1^- \notin S_1 \\ x_2^+ = \Delta_1(x_1^-) & x_1^- \in S_1 \\ \dot{x}_2 = f_2(x_2) + g_2(x_2)u_2 & x_2^- \notin S_2 \\ x_1^+ = \Delta_2(x_2^-) & x_2^- \in S_2 \end{cases}, \tag{12}$$

where $S_1 = \{(q,\dot{q}) \mid z_2(q) = 0,\ \dot{z}_2(q) < 0\}$ is the switching surface, $u_1 = u$, and

$$f_1(x_1) = \begin{bmatrix} \dot{q} \\ D^{-1}(q)(-C(q,\dot{q})\dot{q} - N(q)) \end{bmatrix},$$

$$g_1(x_1) = \begin{bmatrix} 0 \\ D^{-1}(q)B \end{bmatrix},$$

$$x_2^+ = \Delta_1(x_1^-) = \begin{bmatrix} \Delta_q(q^-) \\ \Delta_{\dot{q}}(q^-,\dot{q}^-) \end{bmatrix}. \tag{13}$$

When leg 2 is the support leg, the same derivation produces $S_2 = \{(q,\dot{q}) \mid z_1(q) = 0,\ \dot{z}_1(q) < 0\}$, u_2, $f_2(x_2)$, $g_2(x_2)$ and

$$x_1^+ = \Delta_2(x_2^-). \tag{14}$$

C. Nominal Motion of Walking Along a Straight Line

The legs exchanges roles from one step to the next. If T is the duration of a step, the conditions to ensure walking along a straight line with a symmetric and periodic gait are

$$q_0(t+T) = -q_0(t), \quad q_1(t+T) = -q_1(t)$$
$$q_2(t+T) = q_2(t), \quad q_3(t+T) = q_3(t)$$
$$q_4(t+T) = q_4(t), \quad q_5(t+T) = -q_5(t)$$
$$q_6(t+T) = -q_6(t), \quad q_7(t+T) = q_7(t)$$

and

$$q_8(t+T) = q_8(t). \tag{15}$$

The first condition, $q_0(t+T) = -q_0(t)$, yields a nominal motion along the x-axis of the world frame.

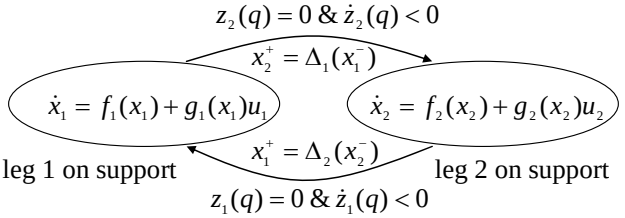

Fig. 3. Bipedal robot's dynamic model as a hybrid system.

D. An Invariance Property of the Model

Let G denote the group of rotations about the z-axis of the world frame, which can be identified with the circle, or $[-\pi,\pi)$. This induces an action on the configuration space Q by $\Phi: G \times Q \to Q$ where $\Phi_g(q) = (q_0 + g, q_1, \ldots, q_8)$. This in turn lifts to an action on the state space TQ by $T\Phi_g(q,\dot{q}) = (\Phi_g(q), \dot{q})$. A function $\psi: TQ \to R^k$, $k \geq 1$, is *invariant* under G if for all $g \in G$ and $(q,\dot{q}) \in Q$, $\psi(\Phi_g(q),\dot{q}) = \psi(q,\dot{q})$ and $F: TQ \to TQ$ is *equivariant* under G if for all $g \in G$ and $(q,\dot{q}) \in TQ$, $F \circ T\Phi_g(q,\dot{q}) = T\Phi_g \circ F(q,\dot{q})$.

Proposition 1: Let $u_1(q,\dot{q})$ and $u_2(q,\dot{q})$ be locally Lipschitz continuous state variable feedbacks and let $x_t(x_0)$ denote a solution of the resulting closed-loop hybrid model (12) with initial condition x_0. If u_1 and u_2 are invariant under G, then $x_t(\cdot)$ is equivariant under G.

The proof is given in Appendix A. In words, the proposition states that if the within-stride feedback controller does not depend on the yaw orientation of the robot (i.e., rotations with respect to the z-axis), then, if the robot is initialized from a given pose and walks for T units of time, and if the initial pose is then rotated by g radians about the z-axis and the robot walks again for T units of time, the two final poses differ by the initial rotation g. This will have a consequence on stability and on the possibility to steer the robot as examined in Section IV - VI.

III. Gait and Within-Stride Controller Design

The nominal gait and controller designs proceed exactly as in [5]. The key steps are summarized here.

A. Virtual Constraints and Within-Stride Controller

The following discussion assumes support on leg 1; a similar discussion applies to leg 2. The discussion also assumes that a direct form of the constraint is used[1]

$$y_{6\times1} = h(q) = q_a - h_d(\theta), \tag{16}$$

where $q_a = [q_3, q_4, \cdots, q_8]^T$ is the vector of actuated coordinates, $\theta = \theta(q)$ is a quantity that is strictly monotonic (i.e., strictly increasing or decreasing) along a typical walking gait, and $h_d(\theta)$ is the desired (asymptotic) evolution of the actuated variables as a function of θ. When the shin and thigh have the same length, the angle of the virtual leg is $\theta = -q_2 - q_3/2$ (the minus sign is used to make θ strictly increasing over a step).

With the direct form of the virtual constraints, the relative

[1] A more general set of virtual constraints is treated in [5].

degree of each component of the output is two, and conditions for the invertibility of the decoupling matrix are easily established as in [22, Prop. 6.1]. The input-output linearizing controller

$$u = u^* - \left(\frac{\partial h}{\partial q} D^{-1} B\right)^{-1} \left(\frac{K_p}{\varepsilon^2} y + \frac{K_d}{\varepsilon} \dot{y}\right), \tag{17}$$

with

$$u^* = \left(\frac{\partial h(q)}{\partial q} D^{-1} B\right)^{-1} \left(\frac{\partial^2 h_d(\theta)}{\partial \theta^2} \dot{\theta}^2(t) + \frac{\partial h(q)}{\partial q} D^{-1}(C(q,\dot{q})\dot{q} + N(q))\right) \tag{18}$$

results in

$$\ddot{y} + \frac{K_d}{\varepsilon} \dot{y} + \frac{K_p}{\varepsilon^2} y = 0 .$$

Appropriate choices for the gains K_p, K_d, and ε allow the errors in the virtual constraints to be driven asymptotically to zero.

Proposition 2: Because the virtual constraints in (16) are invariant under G, the input-output linearizing feedback u in (17) is also invariant under G. If $h_d(\theta)$ is twice differentiable and the second derivative is Lipschitz continuous, then u is Lipschitz continuous.

This is immediate from the expressions for the controller in (17) and (18).

The internal dynamics compatible with the virtual constraints being satisfied, namely,

$$h(q) = q_a - h_d(\theta) = 0, \tag{19}$$

is called the stance phase zero dynamics; the derivation is given in Appendix B. Inspection of (39) shows that the swing phase zero dynamics depend on the choice of the virtual constraint $y = q_a - h_d(\theta) = 0$, but not on how the constraint is zeroed. How to determine a choice for $h_d(\theta)$ that results in a periodic walking motion is summarized next.

B. Constraint Design for Periodic Motion along a Straight Line

The initial state values $x_2^- = (q^-, \dot{q}^-) \in S_2$ are variables that can be freely chosen in the design of a periodic walking motion. First, the initial state for the single-support phase with support on leg 1, $x_1^+ = (q^+, \dot{q}^+) = \Delta_2(x_2^-)$ is calculated. Since a periodic symmetric motion satisfying (15) is desired, the desired final state for the single support on leg 1 is $x_1^- = (H\hat{q}^-, H\dot{\hat{q}}^-)$, in which

$$H = diag\{-1,-1,1,1,1,-1,-1,1,1\} . \tag{20}$$

For simplicity, the virtual constraints $q_a = h_d(\theta)$ are parameterized with cubic polynomials

$$h_d(\theta) = a_3 s^3 + a_2 s^2 + a_1 s + a_0 , \tag{21}$$

where a_3, a_2, a_1 and a_0 are (6×1) coefficient vectors and

$$s = \frac{\theta - \theta_i}{\theta_f - \theta_i} \tag{22}$$

is the normalized independent variable, where $\theta_i = -q_2^+ - q_3^+ / 2$ and $\theta_f = -\hat{q}_2^- - \hat{q}_3^- / 2$ are the initial and final values of θ, respectively. The coefficient vectors a_3, a_2, a_1 and a_0 can be computed to satisfy these boundary conditions. Then the evolution of the unactuated variables $q_u(t)$ is calculated by integration of the dynamic subsystem (39) of the appendix, i.e. the stance phase zero dynamics, starting from the initial state q_u^+ and terminating at $\theta(T) = \theta_f$.

The search for a periodic walking motion is cast as a constrained nonlinear optimization problem and is similar to [5]. It is solved in two stages. In the first stage, a feasible state $x_2^- = (q^-, \dot{q}^-) \in S_2$ is searched. And then in the second stage, an optimal state $x_2^* = (q^-, \dot{q}^-)$ that minimize a given cost criterion, such as energy consumed per step length, is found. The search procedure is carried out in MATLAB with the FMINCON function of the optimization toolbox. A feasible fixed-point solution $x_2^* = (q^-, \dot{q}^-)$ minimizing the cost defines a desired periodic symmetric walking cycle (or nominal orbit).

IV. Stability Analysis

A. Poincaré Map of the Full-model

The stability of a fixed-point x_2^* can be determined by computing the Poincaré map [22, Chap. 4]; here, it will be computed assuming leg-2 is the stance leg, viz $P : S_2 \to S_2$ (called the two-step map). The Poincaré map gives rise to a discrete-time system $x_2(k+1) = P(x_2(k))$ evolving on the switching surface, where as before $S_2 = \{(q,\dot{q}) \mid z_1(q) = 0, \dot{z}_1(q) < 0\}$ is the switching surface and x_2 are the state variables. Because the switching surface S_2 is a hyper surface in R^{18}, the Poincaré map has 17 independent components.

Proposition 3: Under the hypotheses of Propositions 1 and 2, the Poincaré map is equivariant under the action of G, the group of rotations about the z-axis of the world frame. In particular, for each $g \in G$ and $(q,\dot{q}) \in S_2$,

$$P(\Phi_g(q), \dot{q}) = T\Phi_g \circ P(q,\dot{q}) , \tag{23}$$

and hence, if $x^* = (q^*, \dot{q}^*)$ is a fixed point of P, so is $(\Phi_g(q^*), \dot{q}^*)$ for every $g \in G$.

The proof is given in Appendix C. It follows that if the within-stride feedback controller is independent of q_0, periodic orbits cannot be asymptotically stable[2]. At best, they can be asymptotically stable "modulo G". This could be

[2] Asymptotically stable equilibrium points must be isolated; however, Proposition 2 shows that equilibrium points cannot be isolated as they belong to a one-parameter family of equilibrium points corresponding to rotations about the z-axis.

formalized by defining the quotient of the closed-loop hybrid model by G, but this will not be pursued here.

Define a projection operator $\Pi : Q \to S_2$ by

$$\Pi(x_2) = \begin{bmatrix} q_0 & q_1 & q_3 & \cdots & q_8 & \dot{q}_0 & \dot{q}_1 & \cdots & \dot{q}_8 \end{bmatrix}^T,$$

that is, q_2 is eliminated in order to parameterize S_2. The linearization of the Poincaré map about a fixed-point x_2^* gives rise to a linearized system, $\delta x_2(k+1) = A\,\delta x_2(k)$, where $\delta x_2(k) = \Pi(x_2(k) - x_2^*)$ and the (17×17) square matrix A is the Jacobian of the Poincaré map

$$A = \begin{bmatrix} A_0 & A_1 & A_3 & \cdots & A_{17} \end{bmatrix}_{17\times 17}.$$

A fixed-point of the Poincaré map is locally exponentially stable, if and only if the eigenvalues of A have magnitude strictly less than one [22, Chap. 4]. From Proposition 3, we have the following.

Proposition 4: Under the hypotheses of Propositions 1 and 2, the first column of A is given by

$$A_0 = \begin{bmatrix} 1 & 0 & \ldots & 0 \end{bmatrix}^T$$

and hence A always has an eigenvalue at 1.0.

Remark 1: A one-step Poincaré map can also be defined; it requires less computational effort and uses the relationship (15**)** between the natural coordinates for legs 1 and 2. The Poincaré map $P_1 : S_2 \to S_1$ is defined from switching surface S_2 to switching surface S_1, where $S_1 = \{(q,\dot{q}) \mid z_2(q) = 0,\ \dot{z}_2(q) < 0\}$. The ith column of Jacobian of the one-step Poincaré map, $P : S_2 \to S_2$, is obtained as

$$A_i = \Pi\left(\frac{HP_1(x_2^* + \Delta x_i) - HP_1(x_2^* - \Delta x_i)}{2\Delta x_i}\right).$$

In this case, the first column of A is given by $A_0 = \begin{bmatrix} -1 & 0 & \ldots & 0 \end{bmatrix}^T$, and A always has an eigenvalue at -1.0.

B. Hybrid Zero Dynamics (HZD) and the Restricted Poincaré Map

Evaluating the Poincaré map on the full model has a high computational cost. As shown in[22, Chap. 4], the stability test can be evaluated in a reduced-dimensional hybrid zero dynamics. Following [5], the virtual constraints are modified stride-to-stride so that they are compatible with the initial state of the robot at the beginning of each step. The new output for the feedback control design is

$$y_c = h(q, y_i, \dot{y}_i) = q_a - h_d(\theta) - h_c(\theta, y_i, \dot{y}_i). \qquad (24)$$

This output consists of the previous output (16) and a correction term h_c that depends on (16) evaluated at the beginning of the step. Specifically, the function is taken to be a three times continuously differentiable function of θ such that

$$\begin{cases} h_c(\theta_i, y_i, \dot{y}_i) = y_i \\ \dfrac{\partial}{\partial\theta} h_c(\theta_i, y_i, \dot{y}_i) = \dfrac{\dot{y}_i}{\dot{\theta}_i} \\ h_c(\theta, y_i, \dot{y}_i) = 0, \quad 0.5\theta_i + 0.5\theta_f \le \theta \le \theta_f \end{cases} \qquad (25)$$

where the subscript "*i*" denotes the initial value for the current step, and the subscript "*f*" denotes the final value for the current step.

With h_c designed in this ways, the initial errors of the output and its derivative are smoothly joined to the original virtual constraint at the middle of the step. Therefore, for any initial error, the initial virtual constraint h_d is exactly satisfied by the end of the step. Under the new control law defined by (25), the behavior of the robot is completely defined by the impact map and the swing phase zero dynamics (39), where h_d is replaced with $h_d + h_c$. The stability of a fixed point x_2^* can now be tested numerically using a restricted map defined from $S_2 \cap Z$ to $S_2 \cap Z$, where $Z = \{(q,\dot{q}) : y_c(q) = 0, \dot{y}_c(q,\dot{q}) = 0\}$. The key point is that in $S_2 \cap Z$, the state of the robot can be represented using only five independent variables $x^z = \begin{bmatrix} q_0, q_1, \dot{q}_0, \dot{q}_1, \dot{\theta} \end{bmatrix}^T$.

The restricted (two-step) map $P^z : S_2 \cap Z \to S_2 \cap Z$ induces a discrete-time system $x_{k+1}^z = P^z(x_k^z)$. Following [5], and defining $\delta x_k^z = x_k^z - x^{z*}$, the restricted map linearized about a fixed point x^{z*}, $x^{z*} = \begin{bmatrix} q_0^-, q_1^-, \dot{q}_0^-, \dot{q}_1^-, \dot{\theta}^- \end{bmatrix}^T$, gives rise to a linearized system

$$\delta x_{k+1}^z = A^z \delta x_k^z. \qquad (26)$$

From [22, Chap. 4], it can be shown that the restricted map has the same G equivariance properties as the full map. A fixed point of the restricted map is locally exponentially stable, if and only if the eigenvalues of A^z have magnitude strictly less than one [14].

Remark 2: Similar to Remark 1, if a one-step restricted map is used to calculate $P^z(x^{z*} \pm \Delta x_i^z)$, the transformation (15) is applied to the final state of one walking cycle.

V. Walking Along a Straight Line

The physical parameters of the 3D biped used in this study were chosen as in Table I. The parameters result in the center of gravity of the biped being located below the midpoint of the hips.

TABLE I
PARAMETERS FOR THE 3D BIPEDAL ROBOT (in MKS)

W	L_1	L_2	L_3	m_1	m_2	m_3
0.15	0.275	0.275	0.10	0.875	0.875	5.5

A. A Periodic Motion

For these parameters, a periodic orbit was computed following the technique presented in the Section III. We obtained a periodic motion defined by $x_2^* = (q^-, \dot{q}^-)$, where

$x_2^* =$ [0.3151, -0.0838, -0.1317, 0.0997, -0.7543,
0.1948, -0.0592, -1.0471, 0.1809,
-0.1260, 0.2088, -0.8899, 0.3175, 0.0449,
0.5374, -1.5619, 0.9187, 0.6288]'.

Stick diagrams for the first step of the periodic walking gaits are presented in Fig. 4. The walking cycle has a period of $T = 0.4477$ seconds, a step size of $L = 0.0976$ m, and an average walking speed of 0.218 m/sec (or 0.396 body lengths per second). The nominal gait's joint profiles and angular velocities over two consecutive steps are shown in Figs. 5 and 6, respectively. Fig. 7 presents the torque profile required to produce the periodic motion, which is less than 5 N-m for each joint. Fig. 8 shows the profile of the reaction force F_1 on the stance foot and the profile of the swing leg tip; this figure demonstrates that the inequality constraints are satisfied on the nominal motion.

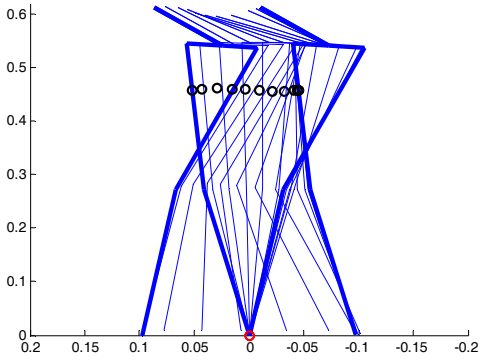

(a) x-z plane (unit:m)

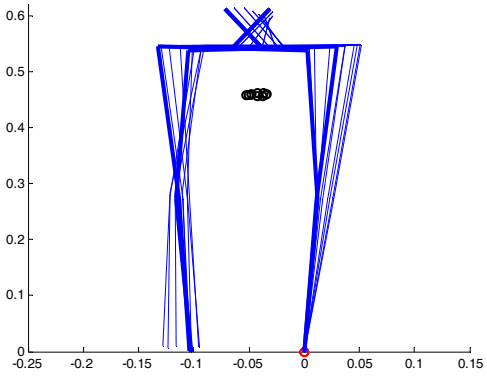

(b) y-z plane (unit:m)

Fig. 4. Stick diagrams for the first step of the periodic walking gait.

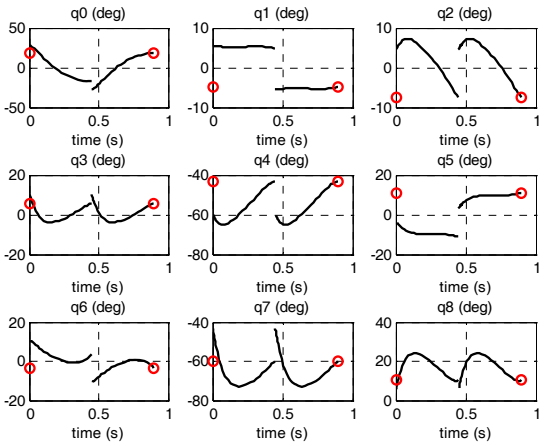

Fig. 5. Joint profiles of the obtained periodic motion over two steps, where the small circles represent q^-. Joint angles q_i, i=0,1,…,8, are shown in the first half in which leg 1 on support, and joint angles q_i, i=0,1,…,8, are shown on the second half in which leg 2 on support.

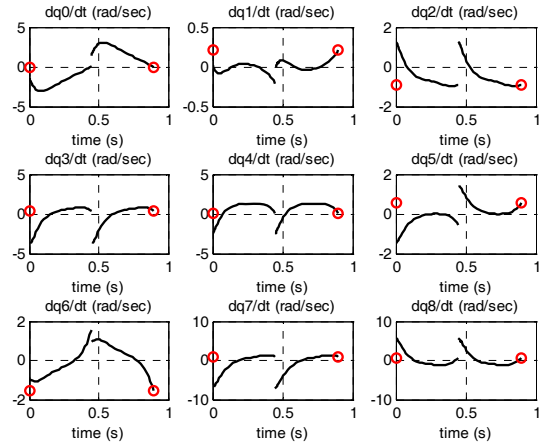

Fig. 6. Joint rate profiles of the obtained periodic motion over two steps, where the small circles represent $\dot{q}^-$. Joint velocities $\dot{q}_i$, i=0,1,…,8, are shown in the first half in which leg 1 on support, and joint velocities $\dot{q}_i$, i=0,1,…,8, are shown on the second half in which leg 2 on support.

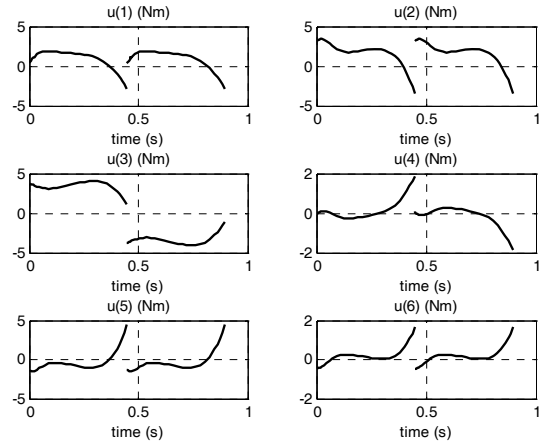

Fig. 7. Torques profiles of the obtained motion over two steps.

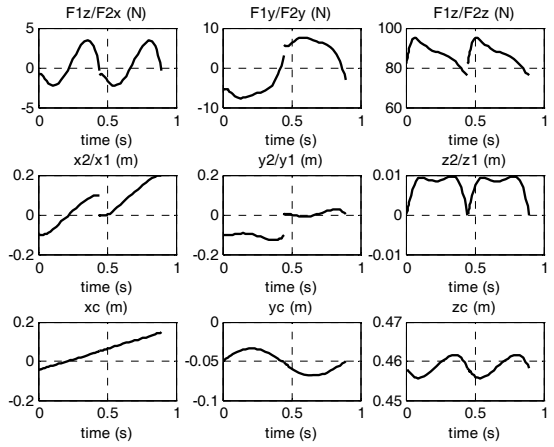

Fig. 8. Reaction force on the stance leg tip over two steps, the evolution of the free tip, and the evolution of the center of mass.

B. *Stability Analysis on the Full Model*

First, the control law (17) for the full model of the 3D biped was used with virtual constraints $y = q_a - h_d(\theta)$; the PD control gains used are $K_p = 50.0$, $K_d = 10.0$ and $\varepsilon = 0.1$. To test the stability of this control law around the periodic motion, the eigenvalues of the linearized Poincaré map A are numerically estimated as in [5] (for $\Delta q_i = 0.0750^\circ$, $\Delta \dot{q}_i = 0.3750^\circ s^{-1}$). The largest eight eigenvalues of the linearized Poincaré maps of the full-model, computed over one step and two-steps, are shown in Table II. As predicted by Proposition 4, the motion is not exponentially stable. However, it is stable for all but the yaw motion of the robot about the stance foot[3].

TABLE II
EIGENVALUES OF FULL-MODE Poincaré MAP A

	one-step map		two-step map	
i	λ_i	$\lvert\lambda_i\rvert$	λ_i	$\lvert\lambda_i\rvert$
1	–1	1	1	1
2	0.8816	0.8816	0.7873	0.7873
3	$0.4057 + j0.7891$	0.8873	$-0.4492 + j0.6287$	0.7727
4	$0.4057 - j0.7891$	0.8873	$-0.4492 - j0.6287$	0.7727
5	–0.5649	0.5649	0.3071	0.3071
6	$-0.0012 + j0.0034$	0.0036	0.0063	0.0063
7	$-0.0012 - j0.0034$	0.0036	0.0014	0.0014
8	0.0010	0.0010	0.0001	0.0001

With virtual constraints $y = q_a - h_d(\theta) - h_c(\theta, y_i, \dot{y}_i)$, the linearization of the one-step restricted Poincaré map was computed, yielding

$$A^z = \begin{bmatrix} -1.0 & -1.0889 & -0.4276 & -0.8996 & 0.3862 \\ 0.0 & 0.8225 & 0.0394 & -0.3344 & -0.5545 \\ 0.0 & 12.4719 & -0.3225 & -3.6756 & -5.3128 \\ 0.0 & 4.4822 & 0.3628 & -0.3943 & -2.3111 \\ 0.0 & -1.4366 & -0.1309 & 0.0039 & 0.9855 \end{bmatrix}.$$

The eigenvalues of the linearized one-step and two-step restricted Poincaré map are shown in Table III.

TABLE III
EIGENVALUES OF HZD RESTRICTED Poincaré MAP A^z

	one-step map		two-step map	
i	λ_i	$\lvert\lambda_i\rvert$	λ_i	$\lvert\lambda_i\rvert$
1	–1	1	1	1
2	0.8781	0.8781	0.7873	0.7733
3	$0.3906 + j0.7766$	0.8693	$-0.4415 + j0.5949$	0.7408
4	$0.3906 - j0.7766$	0.8693	$-0.4415 - j0.5949$	0.7408
5	–0.5681	0.5681	0.3225	0.3225

To illustrate the orbit's local stability of the fixed-point x_2^*, under the continuous controller, a perturbation of $\pi/6$ is added to the initial value of q_0 and very small initial errors are introduced on other joint angles. All joint velocities are also perturbed by very small amounts. The use of small perturbations is due to the fact that the region of attraction is relatively small. Fig. 9 shows the evolution of the final values of the uncontrolled variables (q_0, q_1, q_2) at each step. These variables converge slowly to their desired values except that q_0 moves to an offset value different from the desired ones. Fig. 10 shows phase-plane plots of (q_0, q_1, q_2, θ). The convergence toward a periodic motion is clear for each variable. Note that the value of q_0 does not change signs from one step to the following one; therefore, the robot is following a straight line path that is not aligned with the x-axis of the world frame (the path will be shown in Fig. 16 for comparison with the case of having an additional stride-to-stride controller).

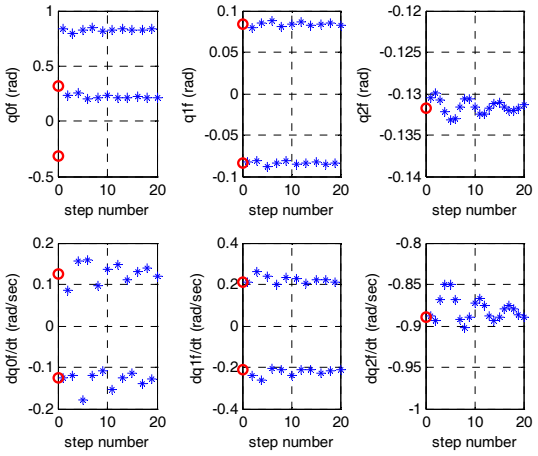

Fig. 9. Evolution of continuous control of unactuated joints (q_0, q_1, q_2) at the end of each step when a perturbation of $\pi/6$ is added to q_0. The small circles represent the values on the desired periodic orbit.

[3] That is, the motion is exponentially stable modulo the symmetry group about the z-axis. As discussed previously, this is the best that can be achieved with a feedback that is yaw invariant.

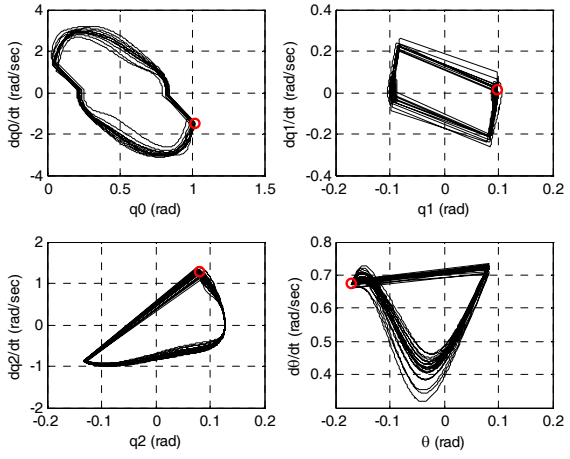

Fig. 10. Phase-plane plots for continuous control (q_0, q_1, q_2, θ) when a perturbation of $\pi/6$ is added on the initial value of q_0. Each variable converges to periodic motion. The small circles represent the initial state.

C. Event-Based Feedback Stabilization of the Nominal Fixed Point

If a desired periodic gait is not exponentially stable or the region of attraction is too small, then event-based stride-to-stride control can be designed and integrated with the continuous, stance-phase controller. Let β be a vector of parameters that are held constant during the stance phase and updated at each impact. Here, it will be updated on the basis of the state of the hybrid zero dynamics. The output (24) is augmented with an additional term,

$$y = q_a - h_d(\theta) - h_c(\theta, y_i, \dot{y}_i) - h_s(\theta, \beta), \tag{27}$$

in which $h_s(\theta, \beta)$ depending on a vector of parameters β, with

$$\begin{cases} h_s(\theta_i, \beta) = 0 \\ \dfrac{\partial h_s}{\partial \theta}(\theta_i, \beta) = 0 \\ h_s(0.5\theta_i + 0.5\theta_f, \beta) = \beta \\ h_s(\theta, \beta) = 0, \quad 0.1\theta_i + 0.9\theta_f \le \theta \le \theta_f \end{cases}. \tag{28}$$

Specifically, $h_s(\theta, \beta)$ is taken to be a fifth-order polynomial for $\theta_i \le \theta \le 0.1\theta_i + 0.9\theta_f$. Continuity of position, velocity, and acceleration is ensured at $\theta = 0.1\theta_i + 0.9\theta_f$.

The restricted Poincaré map can now be viewed as a nonlinear control system on $S_2 \cap Z$ with input β_k, where β_k is the value of β during the step k+1, namely $x^z_{k+1} = P(x^z_k, \beta_k)$. Linearizing this nonlinear system about the fixed point and the nominal parameter value $\beta^* = 0_{6\times1}$ leads to

$$\delta x^z_{k+1} = A^z \delta x^z_k + F \delta \beta_k \tag{29}$$

where $\delta\beta_k = \beta_k - \beta^*$ and F is the Jacobian of the one-step map P^z with respect to β, yielding

$$F = \begin{bmatrix} 0.3107 & -0.0403 & 1.7470 & -1.7910 & -0.5950 & -0.1864 \\ -0.0902 & -0.0815 & -0.1398 & 0.1960 & 0.1502 & 0.0531 \\ 0.7765 & 1.4841 & -1.8355 & 1.8309 & -0.5345 & -0.2104 \\ -0.5933 & -0.6298 & -0.5135 & 0.8142 & 0.8693 & 0.3127 \\ 0.2926 & 0.4204 & -0.0813 & -0.0255 & -0.3829 & -0.1351 \end{bmatrix}. \tag{30}$$

Recall that A^z was defined in Section V-B. Next, design a feedback matrix

$$\delta\beta_k = -K\delta x^z_k, \tag{31}$$

such that the eigenvalues of $(A^z - FK)$ have magnitude strictly less than one. This will exponentially stabilize the fixed point.

To check this, it is enough to verify that for appropriate choice of $h_s(\theta, \beta)$ in (28), the discrete-time system (29) is stabilizable. Then a 6×5 gain matrix K can be calculated via discrete linear quadratic regulator (DLQR) theory, with weighting 1.0 on state x^z and weighting 2.0 on parameters β, to obtain

$$K = \begin{bmatrix} -0.0927 & 0.7069 & -0.0968 & -0.2900 & -0.1286 \\ -0.1066 & 1.1802 & -0.1047 & -0.3310 & -0.1589 \\ -0.1608 & -1.0001 & -0.0452 & 0.1367 & 0.4185 \\ 0.0648 & 2.1802 & 0.0558 & -0.4303 & -0.9764 \\ 0.0835 & 0.2455 & 0.0996 & -0.0336 & -0.4644 \\ 0.0166 & 0.1242 & 0.0370 & -0.0033 & -0.1536 \end{bmatrix}. \tag{32}$$

The eigenvalues of the linearized map with closed-loop stride-to-stride controller are shown in Table IV. All the eigenvalues have magnitude less than 1.0, and thus the obtained nominal orbit x^*_2 is locally exponentially stable. It is noted that the discrete-time system (29) for x^*_1 (i.e. when leg 1 is the support leg) can be written in a similar matter, in which matrices A^z, F, K and the signs of certain entries are modified as shown in Appendix D.

Remark 3: The above stride-to-stride control can also be designed based on the two-step restricted map; however, it was observed in our work that feedback designed on the basis of the one-step restricted map is more effective.

TABLE IV EIGENVALUES OF STRIDE-TO-STRIDE CONTROL

i	λ_i	$\lvert\lambda_i\rvert$
1	0.5248	0.5248
2	$-0.2482 + j0.1723$	0.3077
3	$-0.2482 - j0.1723$	0.3077
4	$0.0890 + j0.2945$	0.3022
5	$0.0890 - j0.2945$	0.3022

To illustrate the orbit's local stability at the fixed-point x^*_2, an initial error of $-1°$ is introduced on each joint and a velocity error of $-3°s^{-1}$ is introduced on each joint velocity. Fig. 11 shows the evolution of the final values of the uncontrolled variables (q_0, q_1, q_2) from one step to the next. These variables converge slowly toward the periodic motion. Fig. 12 shows phase-plane plots of (q_0, q_1, q_2, θ). The convergence toward a

periodic motion is clear for these variables. Fig. 13 shows evolution of the center of mass in the x-y plane, for the 3D biped's full model under closed-loop walking control, with the initial condition perturbed from x_2^*. The value of q_0 is symmetric from one step to the following one; therefore, the robot is following a straight line along the x-axis of the world frame.

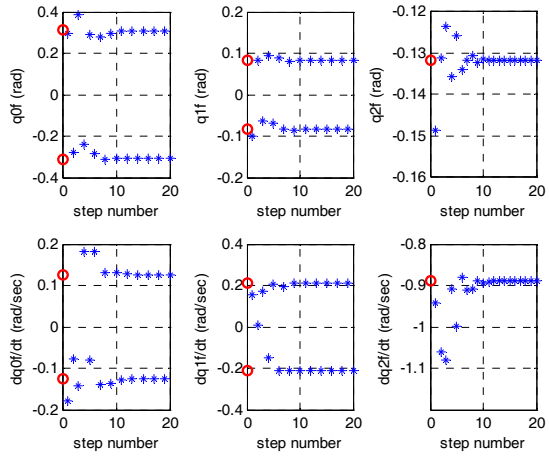

Fig. 11. Evolution of unactuated joints (q_0, q_1, q_2) at the end of each step for the 3D biped's full model under closed-loop walking control, with the initial condition perturbed from x_2^*. The small circles represent the values on the periodic orbit.

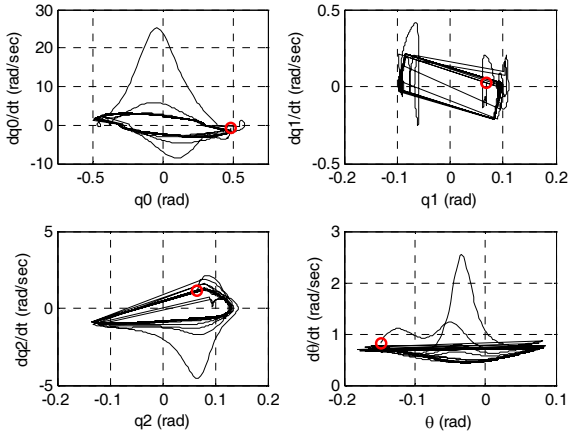

Fig. 12. Phase-plane plots for (q_0, q_1, q_2, θ). The small circles represent the initial state. Each variable converges to a periodic motion.

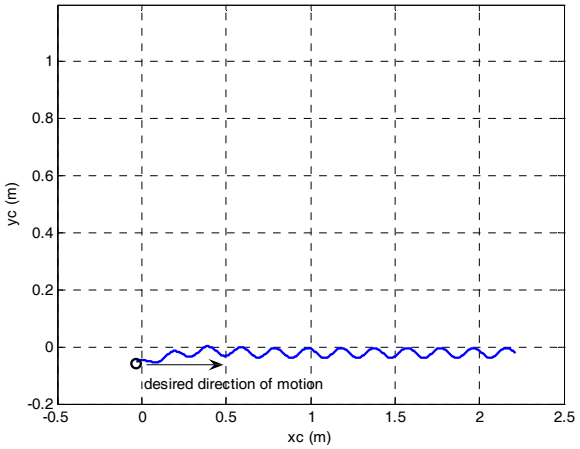

Fig. 13. Evolution of the center of mass in the x-y plane, for the 3D biped's full model under closed-loop walking control, with the initial condition perturbed from x_2^*, where the small circle denotes the starting position.

With the stride-to-stride controller (31), there is no longer an eigenvalue with magnitude one, meaning that the closed-loop system is no longer invariant under rotations by q_0. In particular, the asymptotic value of q_0 will return to the fixed point if an initial error is introduced, which was not the case without the feedback gain *K*. For instance, when a perturbation of $\pi/6$ is added to the initial value of q_0, q_0 converges to the desired value q_0^- quickly. Fig. 14 shows the evolution of the final values of the uncontrolled variables (q_0, q_1, q_2) from one step to the next. These variables converge quickly toward the periodic motion. Fig. 15 shows phase-plane plots of (q_0, q_1, q_2, θ). The convergence toward the periodic motion is also clear for these variables. Fig. 16 shows evolution of the center of mass in the x-y plane, the robot returns within 2% of the desired direction after 3 steps.

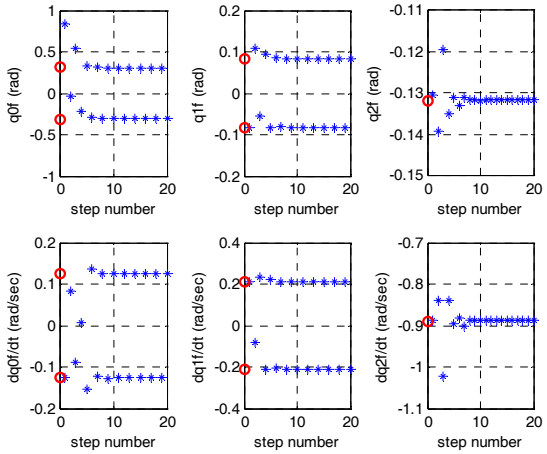

Fig. 14. Evolution of unactuated joints (q_0, q_1, q_2) at the end of each step when a perturbation of $\pi/6$ is added to q_0. The small circles represent the values on the desired periodic orbit.

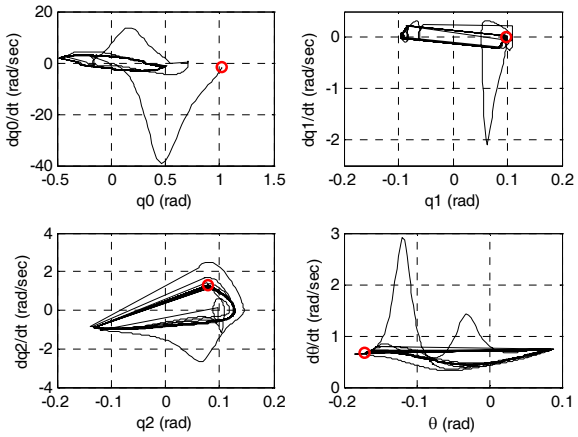

Fig. 15. Phase-plane plots for (q_0, q_1, q_2, θ) when a perturbation of $\pi/6$ is added on the initial value of q_0. Each variable converges to the desired periodic motion. The small circles represent the initial state.

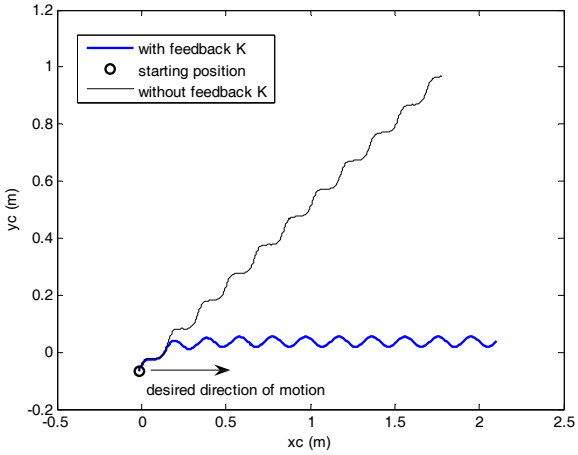

Fig. 16. Evolution of the center of mass in the x-y plane for a perturbation of $\pi/6$ is added on q_0, cases of with and without stride-to-stride feedback control are shown.

VI. Steering Along a Curved Path

This section shows how to add an additional term to the stride-to-stride controller in order to achieve steering along a desired direction. The controller is then modified to achieve steering along a desired path of low curvature.

A. Stride-to-Stride Controller for Controlling Orientation

To plan a turning motion for the bipedal robot, the stride-to-stride controller (31) can be modified as

$$\delta\beta_k = -K(\delta x_k^z - \Delta q_{0cmd}\, e_1),\ e_1 = [1 \quad 0 \quad \cdots \quad 0]^T \qquad (33)$$

where Δq_{0cmd} is a desired (small) amount of relative yaw rotation to be added over the next step. If Δq_{0cmd} is held constant, then the robot's motion will converge to a circular path. If Δq_{0cmd} is slowly varied step to step, then the robot can execute a more complex path. The feedback gain *K* distributes changes to all of the actuated joints as needed for achieving turning.

To induce the 3D point feet bipedal robot to follow a circle in the counter-clockwise direction, the commanded value of q_0^- is incremented by $\Delta q_{0cmd} = 0.1$ rad. at each leg touchdown. Fig. 17 shows the evolution of the final values of the uncontrolled variables (q_0, q_1, q_2) from one step to the next. These variables update automatically to new command values in order to follow a circular path. Fig. 18 shows phase-plane plots of (q_0, q_1, q_2, θ). Fig. 19 shows the evolution of the center of mass in the x-y plane; the radius of the circle is about 1.0 m and it takes 30 seconds to complete one lap of the circle.

It is noted that the closed-loop system is only locally exponentially stable; therefore, a large amount of turning (such as more than 10 degrees in this simulation study) cannot be achieved in one step.

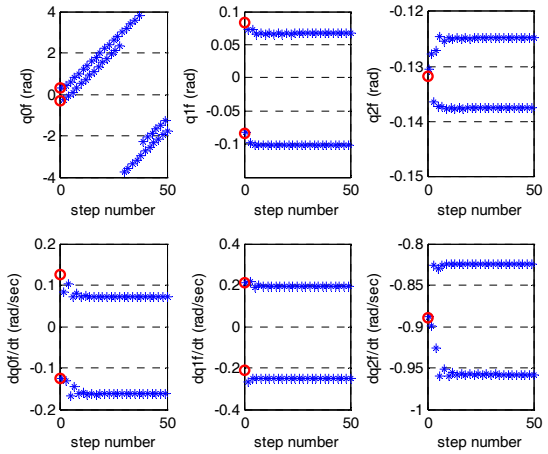

Fig. 17. Evolution of unactuated joints (q_0, q_1, q_2) at the end of each step when the robot changes commanded direction at each step in order to follow a circle .The small circles represent the values on the desired periodic orbit.

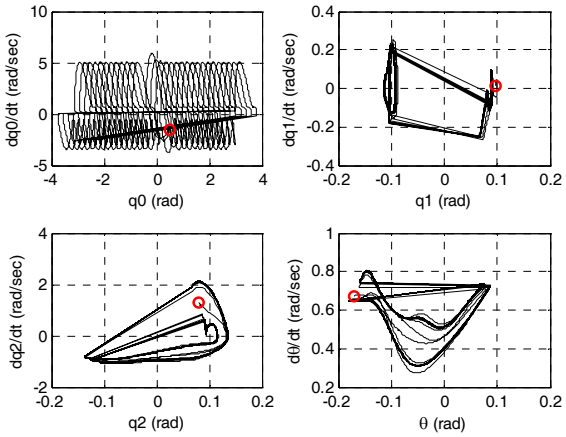

Fig. 18. Phase-plane plots of (q_0, q_1, q_2, θ) when the robot changes commanded direction at each step in order to follow a circle; variable q_0 steps through 360°. The small circles represent the initial state.

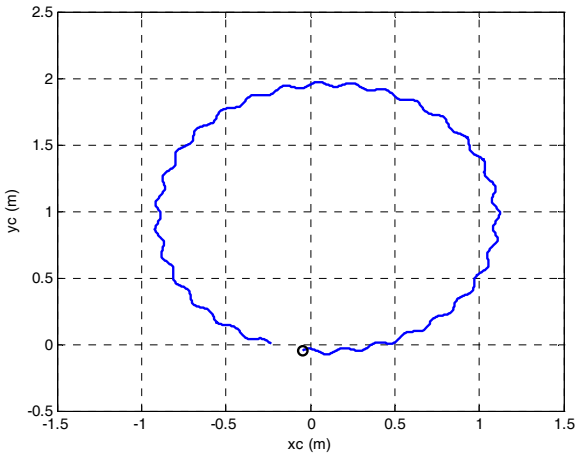

Fig. 19. Evolution of the center of mass in the x-y plane for that the robot changes direction of following a circular path, where the small circle denotes the starting position.

B. Stride-to-Stride Controller for Motion Along a Desired Path in the World Frame

In human walking, it has been observed that, in the majority of turning methods, a person behaves like a nonholonomic vehicle: a lateral step is not used to achieve lateral displacement, rather continuous modification of walking direction (i.e., orientation) is used to produce smooth lateral displacement [2]. Thus it is natural to use the orientation of the robot in order to control its motion along a desired path. In Fig. 16, the stride-to-stride controller (31) can only stabilize the orientation angle of the walking direction but leaves the y-component of the COM (center of mass) uncontrolled. A high-level supervisor control can be integrated into the overall controller to resolve this problem. For example, suppose that it is desired to steer the robot's COM along a path consisting of the world-frame's x-axis, $\theta_{0g} = 0$, with $y = y_g$. A simple strategy to realize this goal is to augment the stride-to-stride control law (31) with an additional proportional correction term δq_0,

$$\delta\beta_k = -K(\delta x_k^z - \delta q_0\, e_1), \tag{34}$$

where

$$\delta q_0 = \begin{cases} Q_0 & k_1(y_g - y_c) > Q_0 \\ -Q_0 & k_1(y_g - y_c) < -Q_0 \\ k_1(y_g - y_c) & otherwise \end{cases},$$

with a proportional gain k_1 and a saturation level Q_0 in order to take into account that the amount of turning that can be realized in one step is limited. Fig. 20 shows the evolution of the COM in the x-y plane for this example (Case 1). The robot not only converges to the orientation angle of the x-axis but also controls its y-coordinate of its COM to within a small range of $y = y_g = 0$. Fig. 21 provides an expanded view of the evolution of the COM.

In the next example, it is desired that the robot move along a path consisting of the world-frame's y-axis, $\theta_{0g} = \frac{\pi}{2}$, at the location of $x = x_g$. With a similar supervisor steering control strategy, the stride-to-stride controller (33) for controlling robot's orientation is also augmented with an additional term as shown below

$$\delta\beta_k = -K(\delta x_k^z - (\Delta q_{0cmd} + \delta q_0)e_1), \tag{35}$$

in which the orientation updating term Δq_{0cmd} is a simple integral control

$$\Delta q_{0cmd} = \begin{cases} Q_0 & k_0(\theta_{0g} - \theta_{0sum}) > Q_0 \\ -Q_0 & k_0(\theta_{0g} - \theta_{0sum}) < -Q_0 \\ k_0(\theta_{0g} - \theta_{0sum}) & otherwise \end{cases},$$

where

$$\theta_{0sum} = \sum \Delta q_{0cmd};$$

and the position correction term δq_0 is a proportional control

$$\delta q_0 = \begin{cases} Q_0 & k_1(x_c - x_g) > Q_0 \\ -Q_0 & k_1(x_c - x_g) < -Q_0 \\ k_1(x_c - x_g) & otherwise \end{cases}.$$

Fig. 20 also shows the evolution of the COM in the x-y plane for the above example (Case 2). The robot not only turns to the orientation angle of the y-axis but also controls the x-coordinate of its COM to within a small range of $x = x_g = 1.0$.

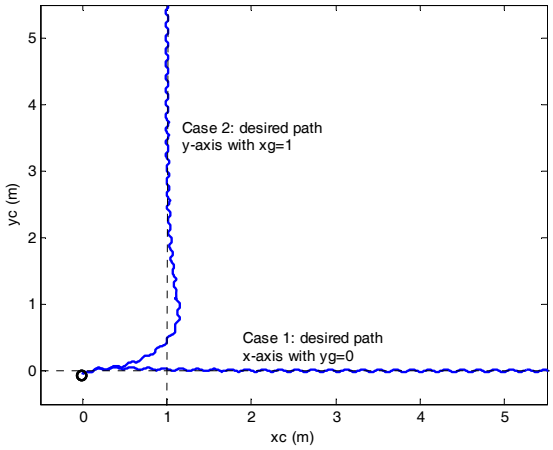

Fig. 20. Evolution of the center of mass in the x-y plane under steering control. Case 1: along a path of the x-axis in the world frame, and Case 2: along a path of the world frame's y-axis at location of x =1. The small circle denotes the starting position and is the same as in Fig. 16.

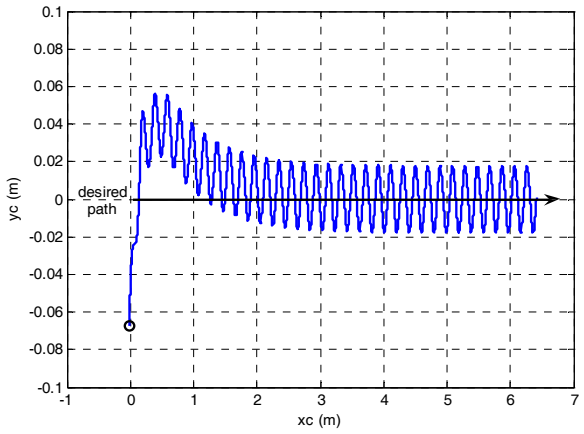

Fig. 21. Enlarged version of Case 1 in Fig. 20.

VII. Conclusion

A 3D point-feet bipedal model has been studied, with the objective of steering the robot in addition to creating an asymptotically stable walking motion. The model assumed rigid links, a passive 3 DoF point contact between the stance leg end and the ground, with all other degrees of freedom actuated. The method of virtual constraints was used to design a time-invariant, within-stride feedback controller that stabilized all but the yaw motion of the robot. A supplemental event-based (or stride-to-stride) feedback controller was then designed that stabilized the yaw motion, resulting in the existence of exponentially stable periodic orbits in the closed-loop hybrid system. Stability was verified through numerical computation of the Jacobian of the Poincaré map. By adjusting the set point of the event-based controller, it was possible to steer the direction of the robot, and even to direct the motion of its center of mass along a given path. This was achieved without designing a new periodic orbit for turning. Instead, by taking advantage of the invariance of the robot dynamics with respect to yaw angle, the controller could be designed on the basis of a single motion designed for walking in a straight line. The event-based controller distributes commands to all of the actuated joints in order to achieve a sufficiently small, desired amount of turning. The restriction on the amount of rotation that can be achieved in a single step arises from the fact that the nominal periodic orbit of the closed-loop system is only locally exponentially stable.

A more energy efficient modification of the actuated joints could probably be proposed if a change in the impact configuration is allowed; this was not studied here. A controller similar to the one developed in this paper is applicable to the model treated in [5], which assumed a passive 2 DoF point contact between the stance leg end and the ground, with no yaw motion. In this case, the change of the yaw angle comes only from the impact phase, when the stance leg changes, and not from the single support phase; nevertheless, a similar strategy of steering control and stability analysis can be developed.

There are several ways in which the result can be extended. To achieve turning with a more aggressive turning rate, solutions of the model can be specifically designed to achieve a large amount of turning in one step. These solutions could then be pieced together as in [23] to achieve maneuvers that steer the robot around obstacles. Treating a model without feet may make it difficult to design controllers that allow the robot to stop, take a step backward and redirect its motion. Hence, another interesting extension of the control strategy developed here is to consider a model with feet, such as in [4, 20].

Appendix

A. Proof of Proposition 1

In [19], it is shown that the kinetic energy term of the Lagrangian model and the impact surfaces are invariant under $SO(3)$, the group of rotations of the world frame, and the impact maps are equivariant under $SO(3)$. Hence, these are in particular invariant and equivariant respectively under G the group of rotations about the z-axis. Because the z-axis of the world frame is aligned with the direction of gravity, the potential energy is invariant under G. From this and the hypothesis on the feedbacks, the vector fields of the closed-loop system are equivariant under G. Putting all of this together, the solutions of the closed-loop system are equivariant.

B. Stance-phase zero dynamics

Let $q_u = [q_0, q_1, \theta]^T$ denote the unactuated joints and $q_a = [q_3, q_4, \cdots, q_8]^T$ denote the actuated joints. A linear relation exists between q and (q_u, q_a),

$$q = E\begin{bmatrix} q_u \\ q_a \end{bmatrix},$$

where E is an (9×9) invertible matrix. Then Eq. (1) can be rewritten as

$$E^T D(q) E\begin{bmatrix} \ddot{q}_u \\ \ddot{q}_a \end{bmatrix} + E^T C(q,\dot{q}) E\begin{bmatrix} \dot{q}_u \\ \dot{q}_a \end{bmatrix} + E^T N(q) = E^T B u \quad (36)$$

and expressed by

$$\begin{bmatrix} D_{11} & D_{12} \\ D_{21} & D_{22} \end{bmatrix}\begin{bmatrix} \ddot{q}_u \\ \ddot{q}_a \end{bmatrix} + \begin{bmatrix} C_{11} & C_{12} \\ C_{21} & C_{22} \end{bmatrix}\begin{bmatrix} \dot{q}_u \\ \dot{q}_a \end{bmatrix} + \begin{bmatrix} N_1 \\ N_2 \end{bmatrix} = \begin{bmatrix} 0_{3\times 1} \\ u_{6\times 1} \end{bmatrix}. \quad (37)$$

The first three lines of the right-hand-side of Eq. (37) are zeros, yielding

$$\left(D_{11}\ddot{q}_u + C_{11}\dot{q}_u + N_1\right) + \left(D_{12}\ddot{q}_a + C_{12}\dot{q}_a\right) = 0_{3\times 1}; \quad (38)$$

and substituting the virtual constraints $q_a = h_d(\theta)$ and

$$\dot{q}_a = \frac{\partial h_d}{\partial \theta}\dot{\theta}, \quad \ddot{q}_a = \frac{\partial h_d}{\partial \theta}\ddot{\theta} + \frac{\partial^2 h_d}{\partial^2 \theta}\dot{\theta}^2,$$

the dynamic model of the single support phase is now reduced to a low-dimensional, 3-DOF, autonomous system

$$\left(D_{11}\ddot{q}_u + C_{11}\dot{q}_u + N_1\right) + \left(D_{12}\frac{\partial h_d}{\partial \theta}\ddot{\theta} + D_{12}\frac{\partial^2 h_d}{\partial \theta^2}\dot{\theta}^2 + C_{12}\frac{\partial h_d}{\partial \theta}\dot{\theta}\right) = 0, \quad (39)$$

which is called the swing phase zero dynamics. It is noted that θ is included in q_u.

C. *Proof of Proposition 3*

The proof is almost immediate from Proposition 1. The Poincaré map is computed by sampling the solution of the model when the swing leg impacts with the ground [22]. From Proposition 1, the solution is equivariant under G. As noted in the proof of Proposition 1, the impact surface is invariant under G, and hence the time-to-impact map is invariant under G. These two facts together prove the proposition.

D. *Discrete-time model for* x_1^*

$$x_1^* = [\,-0.3151,\ 0.0838,\ -0.1317,\ 0.0997,\ -0.7543,\ -0.1948,\ 0.0592,\ -1.0471,\ 0.1809,\ 0.1260,\ -0.2088,\ -0.8899,\ 0.3175,\ 0.0449,\ -0.5374,\ 1.5619,\ 0.9187,\ 0.6288]',$$

$$A^z = \begin{bmatrix} -1.0 & -1.0889 & -0.4276 & -0.8996 & -0.3862 \\ 0.0 & 0.8225 & 0.0394 & -0.3344 & 0.5545 \\ 0.0 & 12.4719 & -0.3225 & -3.6756 & 5.3128 \\ 0.0 & 4.4822 & 0.3628 & -0.3943 & 2.3111 \\ 0.0 & 1.4366 & 0.1309 & -0.0039 & 0.9855 \end{bmatrix}$$

$$F = \begin{bmatrix} -0.3107 & 0.0403 & 1.7470 & -1.7910 & 0.5950 & 0.1864 \\ 0.0902 & 0.0815 & -0.1398 & 0.1960 & -0.1502 & -0.0531 \\ -0.7765 & -1.4841 & -1.8355 & 1.8309 & 0.5345 & 0.2104 \\ 0.5933 & 0.6298 & -0.5135 & 0.8142 & -0.8693 & -0.3127 \\ 0.2926 & 0.4204 & 0.0813 & 0.0255 & -0.3829 & -0.1351 \end{bmatrix}$$

and

$$K = \begin{bmatrix} 0.0927 & -0.7069 & 0.0968 & 0.2900 & -0.1286 \\ 0.1066 & -1.1802 & 0.1047 & 0.3310 & -0.1589 \\ -0.1608 & -1.0001 & -0.0452 & 0.1367 & -0.4185 \\ 0.0648 & 2.1802 & 0.0558 & -0.4303 & 0.9764 \\ -0.0835 & -0.2455 & -0.0996 & 0.0336 & -0.4644 \\ -0.0166 & -0.1242 & -0.0370 & 0.0033 & -0.1536 \end{bmatrix}.$$

REFERENCES

[1] A. D. Ames and R. D. Gregg, "Stably extending two-dimensional bipedal walking to three," *In Proc. of the 2007 American Control Conference*, NY, 20007.

[2] G. Arechavaleta, J-P Laumod, H. Hitcheué, and A. Berthoz, "On the Nonholonomic Nature of Human Locomotion," *Autonomous Robots*, Vol. 25, No. 1-2, pp. 25-35, 2008.

[3] C. Chevallereau, and etc. "RABBIT: A Testbed for Advanced Control Theory," *IEEE Control Systems Magazine*, Vol. 23, No. 5, pp. 57-79, October 2003.

[4] C. Chevallereau, D. Djoudi and J.W. Grizzle, "Stable Bipedal Walking with Foot Rotation Through Direct Regulation of the Zero Moment Point," *IEEE Transactions on Robotics*, Vol. 24, No. 2, pp. 390-401, April, 2008.

[5] C. Chevallereau, J.W. Grizzle and C.-L. Shih, "Asymptotically Stable Walking of a Five-Link Underactuated 3D Bipedal Robot," *IEEE Trans. on Robotics*, Vol. 25, No. 1, pp. 37-50, February 2009.

[6] S. H. Collins, A. Ruina, R. Tedrake, and M. Wisse, "Efficient bipedal robots based on passive-dynamic walkers," *Science*, 307:1082–85, 2005.

[7] T. Fukuda, M. Doi, Hasegawa, and H. Kajima, *Fast Motions in Biomechanics and Robotics*, chapter Multi-Locomotion Control of Biped Locomotion and Brachiation Robot, pp. 121-145, Springer-Verlag, Heidelberg, Germany, 2006.

[8] R.D. Gregg and M.W. Spong, "Reduction-based Control with Application to Three-Dimensional Bipedal Walking Robots," *In Proc. of the 2008 American Control Conference*, Seattle, WA 2008.

[9] J.W. Grizzle, G. Abba, and F. Plestan, "Asymptotically Stable Walking for Biped Robots: Analysis via Systems with Impulse Effects," *IEEE Transactions on Automatic Control*, Vol. 46, pp. 51-46, January 2001.

[10] J.W. Grizzle, ``Remarks on Event-Based Stabilization of Periodic Orbits in Systems with Impulse Effects," *Second International Symposium on Communication, Control and Signal Processing*, March 2006, Marrakech, Morocco.

[11] S. Kazuo, K. Tsuchiya, and K. Tsujita, "Turning Control of a Biped Locomotion Robot using Nonlinear Oscillators," *Proceeding of the 2004 IEEE International Conference on Robotics and Automation*, pp. 3043-3048, New Orleans, LA, April 2004.

[12] A.D. Kuo, "Stabilization of Lateral Motion in Passive Dynamic Walking," *The international Journal of Robotics Research*, Vol. 18, No. 9, pp. 917-930, 1999.

[13] K. Miura, S. Nakaoka, M. Morisawa, K. Harada, and S. Kajita, "A Friction Based Twirl for Biped Robots," *IEEE-RAS International Conference on Humanoid Robots*, pp. 279-284, December, 2008.

[14] B. Morris and J.W. Grizzle, "A Restricted Map for Determining Exponentially Stable Periodic Orbits in Systems with Impulse Effects: Application to Bipedal Robots," *2005-CDC*, Seville, Spain, Dec. 2005.

[15] F. Plestan, J. W. Grizzle, and E.R. Westervelt, and G. Abba, "Stable Walking of a 7-DOF Biped Robot," *IEEE Transactions on Robotics and Automation*, Vol. 19, No. 4, pp. 653-668, August 2003.

[16] Y. Sakagami, R. Watanabe, C. Aoyama, S. Matsunaga, N. Higaki, and K. Fulimura, "The intelligent ASIMO system overview and integration," *Proceeding of the 2002 IEEE/RSJ International Conference on Intelligent Robots and Systems*, pp. 2478-2483, EPFL Lausanne, Suisse, 2002.

[17] C.L. Shih, J.W. Grizzle, and C. Chevallereau, "Asymptotically Stable Walking of a Simple Underactuated 3D Bipedal Robot," *The 33rd Annual Conference of the IEEE Industrial Electronics Society* (*IECON*), pp.2766-2771, Taipei, Taiwan, November, 2007.

[18] G. Song and M. Zefran, "Underactuated Dynamic Three-Dimensional Bipedal Walking," *Proceeding of the 2006 IEEE International Conference on Robotics and Automation*, Orlando, Florida, May 2006, pp. 854-859.

[19] M.W. Spong and F. Bullo, "Controlled Symmetries and Passive Walking," *IEEE Transactions on Automatic Control*, Vol. 50, No. 7, pp: 1025-1031, July, 2005.

[20] M. Vukobratovic, B. Borovac, and V. Potkonjak, " ZMP: A Review of Some Basic Misunderstandings," *International Journal of Humanoid Robotics*, Vol. 3, No. 2, pp. 153-175, June 2006.

[21] E.R. Westervelt, J.W. Grizzle, and D.E. Koditschek, "Hybrid Zero Dynamics of Planar Biped Walkers," *IEEE Transaction on Automatic Control*, Vol. 48, No. 1, pp. 42-56, January 2003.

[22] E.R. Westervelt, J.W. Grizzle, C. Chevallereau, J. Choi, and B. Morris, *Feedback Control of Dynamic Bipedal Locomotion* (*Control and Automation*) ,Boca Raton FL: CRCPress, June 2007.

[23] E.R. Westervelt, J.W. Grizzle, and C. Canudas de Wit, "Switching and PI Control for Planar Biped Walkers," *IEEE Transactions on Automatic Control*, Vol. 48, No. 2, pp. 308-312, February 2003.

[24] M. Yagi and V. Lumelsky, "Synthesis of Turning Pattern Trajectories for a Biped Robot in a Scene with Obstacles," *Proceedings of the 2000 IEEE/RSJ International Conference on Intelligent Robots and Systems*, pp. 1161-1166, 2000.

[25] R. D. Gregg and M. W Spong, **"**Reduction-Based Control of Three-Dimensional Bipedal Walking Robots," *IJRR*, to appear. Pre-print available at http://ijr.sagepub.com/cgi/content/abstract/0278364909104296v1

[26] R. D. Gregg and M. W Spong, **"**Reduction-Based Control of Branched Chains: Application to Three-Dimensional Bipedal Torso Robots." Submitted to the *2009 IEEE Conference on Decision and Control*, Shanghai, China.

[27] R. D. Gregg and M. W Spong, **"**Bringing the Compass-Gait Bipedal Walker to Three Dimensions." Submitted to the *2009 International Conference on Intelligent Robots and Systems*, St. Louis, MO.

[28] A. D. Ames, R. D. Gregg, E. D. B. Wendel and S. Sastry, "On the Geometric Reduction of Controlled Three-Dimensional Robotic Bipedal Walkers," In F. Bullo and K. Fujimoto, editors, *Lagrangian and Hamiltonian Methods for Nonlinear Control 2006*, volume 366/2007 Lecture Notes in Control and Information Sciences, pp.183-196. Springer-Verlag, 2007.

[29] A. D. Ames, R. D. Gregg and M. W. Spong, "A Geometric Approach to Three-Dimensional Hipped Bipedal Robotic Walking," *In 46th IEEE Conference on Decision and Control, New Orleans*, LA, 2007.

[30] A. D. Ames, R. Sinnet and E. Wendel, "Three-dimensional Kneed Bipedal Walking: A Hybrid Geometric Approach," In P. Tabuada and R. Majumdar, editors, *Hybrid Systems: Computation and Contro*l, volume 5469 Lecture Notes in Computer Science, pp. 16-30. Springer-Verlag, 2009.

[31] R. Sinnet and A. D. Ames, "2D Bipedal Walking with Knees and Feet: A Hybrid Control Approach," Submitted to *CDC, 2009*.

[32] R. Sinnet and A. D. Ames, "3D Bipedal Walking with Knees and Feet: A Hybrid Geometric Approach," Submitted to *CDC, 2009*.